Computational capacity of pyramidal neurons in the cerebral cortex

Danko D. Georgiev[a,*], Stefan K. Kolev[b], Eliahu Cohen[c], James F. Glazebrook[d]

[a]*Institute for Advanced Study, 30 Vasilaki Papadopulu Str., Varna 9010, Bulgaria*
[b]*Institute of Electronics, Bulgarian Academy of Sciences, 72 Tzarigradsko Chaussee Blvd., Sofia 1784, Bulgaria*
[c]*Faculty of Engineering and the Institute of Nanotechnology and Advanced Materials, Bar Ilan University, Ramat Gan 5290002, Israel*
[d]*Department of Mathematics and Computer Science, Eastern Illinois University, Charleston, IL 61920, USA*

Abstract

The electric activities of cortical pyramidal neurons are supported by structurally stable, morphologically complex axo-dendritic trees. Anatomical differences between axons and dendrites in regard to their length or caliber reflect the underlying functional specializations, for input or output of neural information, respectively. For a proper assessment of the computational capacity of pyramidal neurons, we have analyzed an extensive dataset of three-dimensional digital reconstructions from the NeuroMorpho.Org database, and quantified basic dendritic or axonal morphometric measures in different regions and layers of the mouse, rat or human cerebral cortex. Physical estimates of the total number and type of ions involved in neuronal electric spiking based on the obtained morphometric data, combined with energetics of neurotransmitter release and signaling fueled by glucose consumed by the active brain, support highly efficient cerebral computation performed at the thermodynamically allowed Landauer limit for implementation of irreversible logical operations. Individual proton tunneling events in voltage-sensing S4 protein α-helices of Na^+, K^+ or Ca^{2+} ion channels are ideally suited to serve as single Landauer elementary logical operations that are then amplified by selective ionic currents traversing the open channel pores. This miniaturization of computational gating allows the execution of over 1.2 zetta logical operations per second in the human cerebral cortex without combusting the brain by the released heat.

Keywords: action potential, brain energetics, logical operation, morphometry, pyramidal neuron

1. Introduction

The cerebral cortex is the seat of higher cognitive functions in mammals. Structurally, it is divided into neocortex, made up of six layers of neurons, and allocortex, made up of just three or four layers of neurons (Rockland & DeFelipe, 2018). The neocortex forms the largest, outer layer of the cerebrum. In large mammals and primates, the neocortex is folded into grooves and ridges, which minimize the brain volume, and are pivotal for the wiring of the brain and its functional organization (Rakic, 2009). The neocortex is involved in sensory perception, awareness, attention, motor control, working memory, thought, intelligence, and consciousness (Page, 1981). The allocortex includes evolutionary older regions, such as the olfactory system and the hippocampus, which comprise the neural basis of emotion and play important roles in time ordering of memorized events or the consolidation of conscious memory from short-term to long-term memory (Fournier et al., 2015; Squire et al., 2015; Wible, 2013).

Excitatory, glutamatergic pyramidal neurons are the principal type of cell comprising over 70% of all cortical neurons (Nieuwenhuys, 1994). Pyramidal neurons, referred to as the "psychic cells" of the brain by Ramón y Cajal (Goldman-Rakic, 2002), are organized in complex neuronal networks, which communicate

---

*Corresponding author

Email addresses: `danko.georgiev@mail.bg` (Danko D. Georgiev), `kolevskk@abv.bg` (Stefan K. Kolev), `eliahu.cohen@biu.ac.il` (Eliahu Cohen), `jfglazebrook@eiu.edu` (James F. Glazebrook)

by means of electric signals. Wiring of the corresponding neuronal networks requires individual neurons to support structurally stable, elongated cable-like projections referred to as *neurites*. Depending on their functional specialization, the neurites could be classified as dendrites, specialized in delivering inputs to the neuron, or axons, specialized in delivering outputs from the neuron to other neurons (Georgiev, 2017). Dendrites deliver electric signals through activated synapses mainly formed onto spines of the dendritic tree (Eyal et al., 2018). The post-synaptic electric currents propagate passively along the dendrites through an electrotonic mechanism that summates the electric signals spatially and temporally at the cell body (soma) of the neuron. Axons output electric spikes (action potentials) in an active fashion that consumes large amounts of biochemical energy in order to propagate the electric signals without attenuation at a distance to pre-synaptic axonal buttons whose release of neurotransmitter subsequently affects the electric properties of dendrites of target neurons.

The morphology of neurites is intimately related to their characteristic functional role (Mounier et al., 2015). Dendrites achieve processing of received information through passive and lossy transmission. Consequently, the dendrites have shorter lengths and larger diameters in order to compensate for the electrotonic attenuation of currents with distance. Alternatively, axons are required to deliver output signals at large distances to target neurons through lossless transmission achieved at the expense of biochemical energy. To reduce energy expenditure, axons are thinner and insulated with myelin sheets. Thus, a detailed study of neuronal morphology is essential for better understanding of the neuronal hardware behind higher cognitive functions.

Here, we analyze a dataset of 749 three-dimensional neuronal reconstructions from NeuroMorpho.org 7.8 digital archive (Ascoli et al., 2007). Then, with the use of morphometric, electrophysiological and biochemical data, we derive an upper bound on the computational capacity of pyramidal neurons in the cerebral cortex. Finally, we conclude with a theoretical discussion on the fundamental limitations imposed by energetics on possible subneuronal mechanisms for the processing of cognitive information.

2. Results

2.1. Dendrite morphometry

Pyramidal neurons are located within layers 2, 3, 5 and 6 of the neocortex (Shipp, 2007). The cell body (soma) of pyramidal neurons has the shape of a pyramid with its base facing towards the deeper layers and its apex towards the superficial layers of the cerebral cortex (Bekkers, 2011). Because the dendrites of pyramidal neurons from layers 2, 3 and 5 reach layer 1, the size and complexity of their dendritic trees increases with the depth of the neuron within the cortex. In contrast, the dendrites of layer 6 neurons reach only layer 4, which explain why their dendritic trees are smaller and less complex than layer 5 neurons (Figure 1). On average across all types of cortical pyramidal neurons, the basal dendrites have $\approx 33.6\%$ shorter total length (3513 ± 2199 μm) in comparison to apical dendrites (5295 ± 3524 μm) ($F_{1,737} = 73.0$, $P < 0.001$, Figure 2a). The mean radius of basal dendrites is also $\approx 14.0\%$ thinner (0.54 ± 0.40 μm) compared to apical dendrites (0.63 ± 0.40 μm) ($F_{1,737} = 30.8$, $P < 0.001$, Figure 2b), which results in $\approx 47.6\%$ lower total volume of basal dendrites (5881 ± 14897 μm^3) as opposed to apical dendrites (11231 ± 29236 μm^3) ($F_{1,737} = 5.7$, $P = 0.017$, Figure 2c). Detailed morphometric data for basal and apical dendrites in neocortex, subiculum or hippocampus of mouse, rat and human are presented in Table 1 and Table 2.
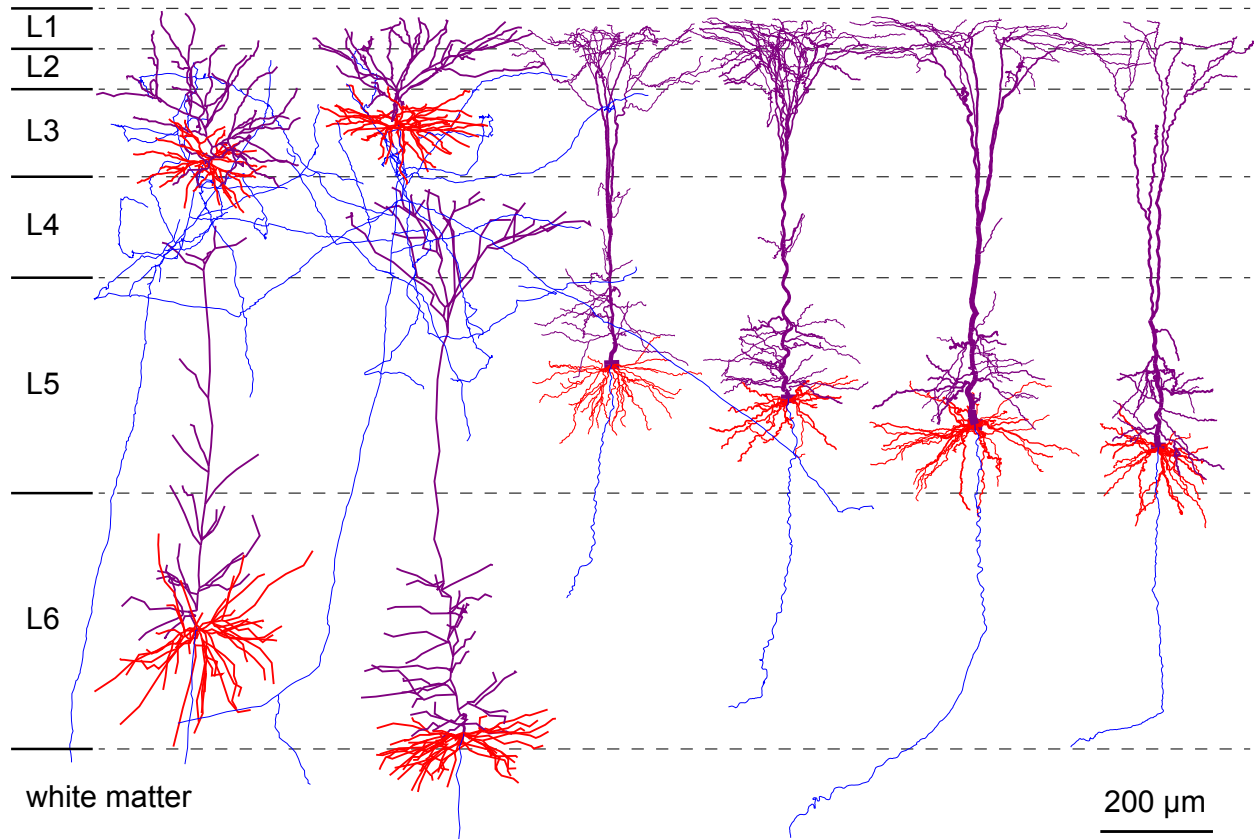
2

Figure 1: Layered structure of mouse neocortex constructed in silico with digital reconstructions of Layer 2-3 pyramidal neurons (NMO_51117, NMO_51116), Layer 5 pyramidal neurons (NMO_09483, NMO_09485, NMO_09480, NMO_09494) and Layer 6 pyramidal neurons (NMO_85158, NMO_85162). Basal dendrites are rendered in red, apical dendrites in purple, and axons in blue. Neuron identification numbers are given from left to right of the rendered reconstructions.

2.2. Axon morphometry

Axons are specialized to deliver electric output to distant targets. The mean radius of axons (0.45 ± 0.34 μm) is $\approx 25\%$ thinner compared to the mean radius of dendrites (0.60 ± 0.39 μm) (paired t-test, $t_{1,527} = 10.3$, $P < 0.001$, Figure 2e) estimated in a subset of 528 cells, which had either partial axonal arborizations in slices ($n = 370$) or complete axonal arborizations in whole brain reconstructions ($n = 158$). The rationale for this analysis is that slicing does not affect the radii of neuronal projections. However, because the axonal arborizations are trimmed in slice sections, for the evaluation of total axonal length and total axonal volume, we have used only the subset of 158 automated whole brain reconstructions in mouse (Table 3). Axons of mouse projection neurons have $\approx 10.8\times$ greater total length (79020 ± 81159 μm) and $\approx 8.1\times$ greater total volume (137351 ± 193481 μm^3) in comparison with dendrite total length (7319 ± 4079 μm) (paired t-test, $t_{1,157} = 11.5$, $P < 0.001$, Figure 2d) and total volume (16862 ± 14656 μm^3) (paired t-test, $t_{1,157} = 8.1$, $P < 0.001$, Figure 2f).

2.3. Energetics of the cerebral cortex

Approximately 20% of resting oxygen consumption (i.e. in the absence of heavy physical work by skeletal muscles) is absorbed by the human brain (Laughlin et al., 1998). Brain activity is fueled almost exclusively by glucose (Magistretti & Allaman, 2015). Oxidative metabolism in mitochondria of 1 glucose molecule leads to the production of 32 ATP molecules (Mergenthaler et al., 2013), each of which releases 0.4 eV of free energy upon hydrolysis (George et al., 1970; Scott, 2005). Thus, the free energy available for utilization by
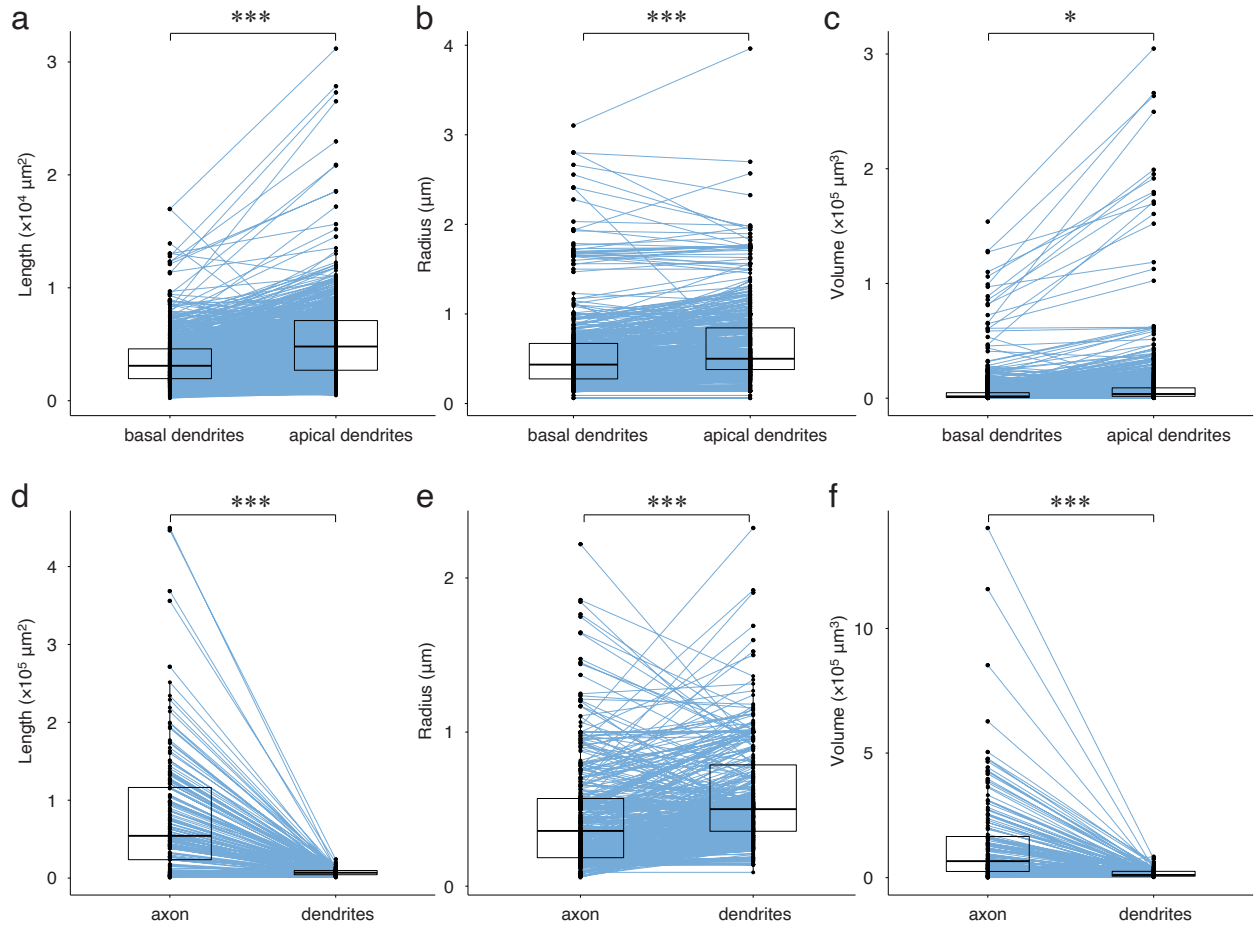
3

Figure 2: Paired box plots for morphometric measures in cortical pyramidal neurons. Comparison of total length L, average radius r, and total volume $V = \pi r^2 L$ was performed for basal dendrites versus apical dendrites (a-c) or axon versus dendrites (d-f). Individual measurements are represented with black dots. Paired measurements performed in the same cell are connected with thin blue lines. The bottom and the top of each box represent the lower ($Q1$) and upper ($Q3$) quartile, whereas the black line in the middle of the box represents the median. The interquartile range (IQR $= Q3 - Q1$) contains the middle 50 % of the data, the whiskers extending from the minimum $Q1 - 1.5 \times$IQR to the maximum $Q3 + 1.5 \times$IQR value indicate the spread of the data, and the outliers are represented by data points that are located outside the whiskers of the box plot. Statistical significance was estimated by repeated-measures analysis of variance (rANOVA): *, $p < 0.05$; ***, $p < 0.001$.

neuronal activities from glucose is only 1235 kJ/mol, even though combustion of glucose in oxygen releases 2801 kJ/mol. From the speeds of glucose consumption (Herculano-Houzel, 2011) by the cerebral cortex of different species (Table 4), it can be estimated that the power of the mouse cortex is 0.004 W, rat cortex is 0.015 W, and human cortex is 4.427 W. These cortical values comprise approximately half of the power of the whole brain (Table 5), namely, the power of the mouse brain is 0.008 W, rat brain is 0.025 W, and human brain is 9.628 W. This modest consumption of energy points to highly efficient energy utilization, and miniaturization of the brain's logical circuitry.

2.4. Computational capacity of pyramidal neurons

Pyramidal neurons input, process and output cognitive information with the use of electric spikes. There are five main physiological processes that support each spike (Figure 3a):

(1) Each neuron needs multiple excitatory dendritic inputs, which activate post-synaptic neurotransmitter receptors and generate excitatory post-synaptic potentials (EPSPs).

4

Table 1: Morphometric measures for basal dendrites of pyramidal neurons.

Species	Brain region	Neuron type	# of cells	Total length (μm)	Total volume (μm^3)	Mean radius (μm)
Mouse	Neocortex	Layer 2-3	15	3398 ± 1638	8138 ± 6050	0.84 ± 0.23
		Layer 5	156	3433 ± 2439	5702 ± 8551	0.64 ± 0.40
		Layer 6	37	3728 ± 1773	8058 ± 6309	0.79 ± 0.24
	Hippocampus	CA1	20	2342 ± 755	3568 ± 5430	0.59 ± 0.27
	Subiculum	Principal	24	3192 ± 1081	4179 ± 3305	0.62 ± 0.20
Rat	Neocortex	Layer 2-3	125	2086 ± 1120	850 ± 1122	0.32 ± 0.15
		Layer 5	171	4854 ± 2416	11473 ± 26126	0.60 ± 0.39
		Layer 6	20	1966 ± 445	531 ± 290	0.28 ± 0.06
	Hippocampus	CA1	113	2955 ± 1364	5255 ± 14778	0.50 ± 0.64
		CA3	62	4358 ± 2166	3036 ± 4122	0.44 ± 0.23
Human	Neocortex	Layer 2-3	6	8220 ± 1153	10453 ± 2079	0.64 ± 0.04

Table 2: Morphometric measures for apical dendrites of pyramidal neurons.

Species	Brain region	Neuron type	# of cells	Total length (μm)	Total volume (μm^3)	Mean radius (μm)
Mouse	Neocortex	Layer 2-3	15	3470 ± 1735	8463 ± 6775	0.83 ± 0.24
		Layer 5	156	4067 ± 2503	6512 ± 7853	0.69 ± 0.37
		Layer 6	37	3622 ± 1715	7691 ± 5640	0.79 ± 0.24
	Hippocampus	CA1	20	3821 ± 1119	6658 ± 8380	0.67 ± 0.26
	Subiculum	Principal	24	3130 ± 1591	4276 ± 4812	0.61 ± 0.21
Rat	Neocortex	Layer 2-3	125	2418 ± 1192	1471 ± 2028	0.39 ± 0.20
		Layer 5	171	8393 ± 4638	28280 ± 52456	0.78 ± 0.45
		Layer 6	20	3947 ± 1360	1767 ± 786	0.38 ± 0.11
	Hippocampus	CA1	113	6517 ± 1903	10939 ± 27586	0.57 ± 0.57
		CA3	62	6228 ± 1940	6170 ± 5512	0.54 ± 0.24
Human	Neocortex	Layer 2-3	6	9163 ± 1588	12488 ± 4609	0.65 ± 0.07

Table 3: Morphometric measures for axons of pyramidal neurons.

Species	Brain region	Neuron type	# of cells	Total length (μm)	Total volume (μm^3)	Mean radius (μm)
Mouse	Neocortex	Layer 2-3	15	65749 ± 49489	95778 ± 41755	0.75 ± 0.23
		Layer 5	81	87865 ± 103291	165888 ± 250718	0.72 ± 0.23
		Layer 6	37	86886 ± 51082	131152 ± 107960	0.67 ± 0.22
	Hippocampus	CA1	1	24677	20412	0.51
	Subiculum	Principal	24	47600 ± 25061	81450 ± 98365	0.64 ± 0.20

(2) EPSPs propagate towards the soma where they summate to reach a certain voltage threshold and trigger an action potential at the axonal hillock. The action potential then propagates to pre-synaptic axonal buttons that innervate target neurons.

(3) To excite the target neurons, the pre-synaptic electric spike is temporarily converted into chemical signal through exocytosis of synaptic vesicles that release excitatory neurotransmitter such as glutamate or aspartate.

(4) The excess neurotransmitter is recycled by glial cells. Glial cells also support neuronal homeostasis by controlling the chemical contents of the extracellular matrix.

(5) In between spikes, both pyramidal neurons and glial cells expend energy in order to maintain their

Table 4: Energy consumption by neurons in the cerebral cortex.

Species	Cortical mass (gray + white matter) (g)	Glucose use per gram per minute (μmol/g·min)	Total number of cortical neurons ($\times 10^7$)	Energy use per neuron (pW)	Total energy use by cortex (W)
Mouse	0.173	1.10	1.369	286.13	0.004
Rat	0.769	0.95	3.102	484.77	0.015
Human	632.52	0.34	1634	270.91	4.427

Table 5: Energy consumption by neurons in the brain.

Species	Brain mass (g)	Glucose use per gram per minute (μmol/g·min)	Total number of brain neurons ($\times 10^7$)	Energy use per neuron (pW)	Total energy use by brain (W)
Mouse	0.416	0.89	7.089	107.50	0.008
Rat	1.802	0.68	20.013	126.03	0.025
Human	1508.91	0.31	8606	111.88	9.628

resting membrane potentials and to restore the initial concentration gradients of Na^+, K^+ or Ca^{2+} ions.

The energy expenditure *in vivo* varies from neuron to neuron depending on the exact morphometric measures and physiological activities. However, it is possible to estimate the energy budget for an average cortical pyramidal neuron under the assumption that all of the energy released from glucose consumed by the brain cortex is used to fuel electric spiking with the underlying biomolecular processes. Because the maintenance of resting membrane potential by neurons, and the accompanying glial support could be viewed as continuous processes interspersed by discrete action potentials, the general outline of the calculation of the energy budget per spike is as follows: Firstly, from the total energy budget of the cerebral cortex, the energy needed for neuronal resting membrane potential and glial support is subtracted. Secondly, from the remaining energy, the maximal average frequency of firing electric spikes is computed. Thirdly, the maximal average firing frequency provides an estimate of the duration of the average interspike interval and the corresponding energy expenditure for the neuronal resting membrane potential and glial support per single spike. Finally, the data so obtained will be integrated for calculating the total energy expenditure to support a single spike together with its preceding interspike interval.

2.4.1. Resting membrane potential

Physiological electric activities are due to passage of metal ions across the plasma membrane. The resting membrane potential of neurons is approximately -70 mV. The influx of Na^+ ions leads to depolarization, whereas the efflux of K^+ ions leads to hyperpolarization of the transmembrane voltage. Neurons use 3.42×10^8 ATP molecules per second in order to keep steady their resting membrane potential (Attwell & Laughlin, 2001). The power consumed by 1.634×10^{10} neurons in the human cerebral cortex (Herculano-Houzel, 2011) for their resting potential is 0.358 W, which accounts for $\approx 8.1\%$ of the total cortical power.

2.4.2. Glial support

Glial cells also spend energy to sustain their resting membrane potential at about -60 mV (McKhann et al., 1997). Glial cells, which are $3.8\times$ more numerous than neurons in the cerebral cortex (Azevedo et al., 2009), consume 1.02×10^8 ATP molecules per glial cell each second (Attwell & Laughlin, 2001). For the human cerebral cortex, the energy consumption by glial cells is 0.406 W, which constitutes $\approx 9.2\%$ of the total cortical power.
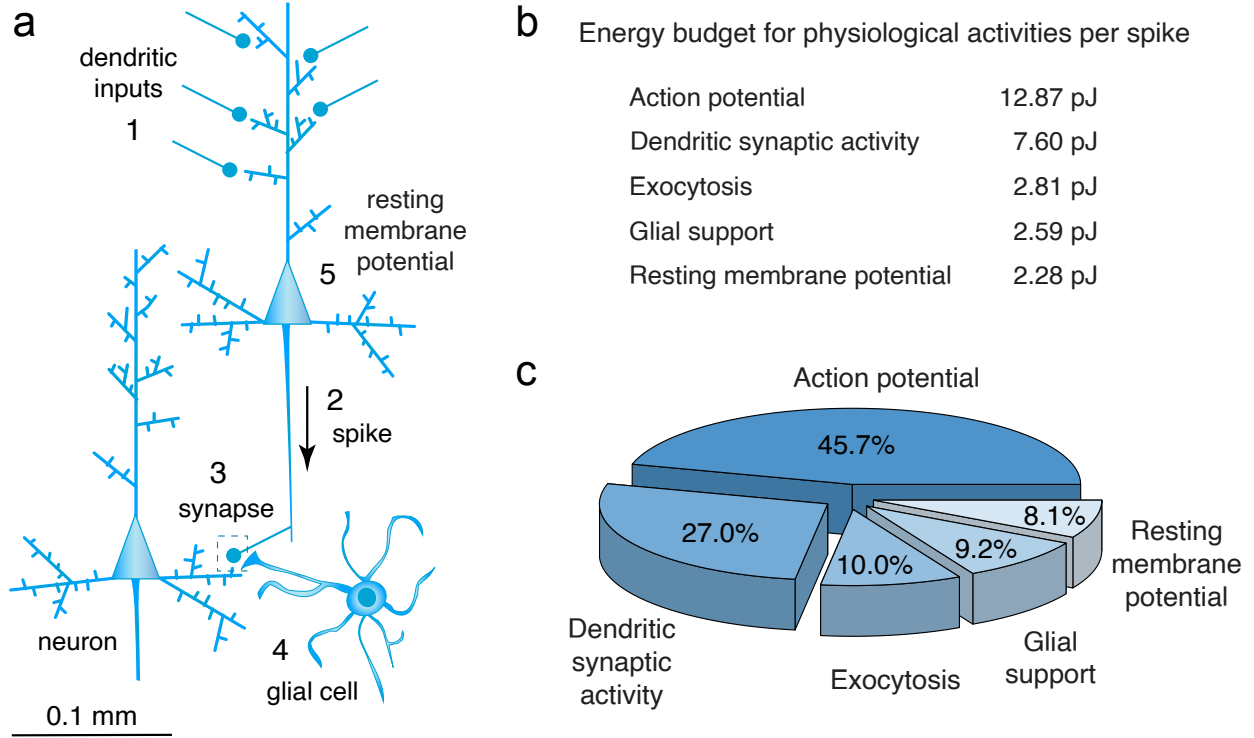
Figure 3: Physiological activities underlying the input, processing and output of cognitive information through electric spikes by pyramidal neurons. (a) To generate an electric spike, each neuron (1) needs multiple excitatory dendritic inputs, which activate post-synaptic neurotransmitter receptors. The excitatory post-synaptic potentials (EPSPs) then (2) summate at the soma and trigger an action potential at the axonal hillock. The action potential propagates to pre-synaptic axonal buttons that (3) release neurotransmitter through exocytosis of synaptic vesicles. Excess neurotransmitter is (4) recycled by glial cells, which support the proper functioning of neurons. In between spikes, pyramidal neurons expend energy in order to (5) maintain their resting membrane potential. The energy budget in picojoules (pJ) for these five main physiological activities per spike is tabulated in (b) and displayed as a pie chart with percentages of the total energy consumed in (c).

2.4.3. Action potentials

Neuronal dendrites are unmyelinated and leak-prone, but they need to be depolarized in their proximal part that is adjacent to soma, to a level slightly above a threshold of -54 mV (Pathak et al., 2016) in order to trigger an action potential at the axonal hillock. To reduce leakage, and achieve efficient transport of the electric spike to distant targets, the axons are myelinated with the exception of the nodes of Ranvier, where upon electric stimulation, the membrane readily depolarizes to $+40$ mV due to opening of voltage-gated Na^+ channels. The number of Na^+ ions entering into a cylindrical neurite segment is given by the capacitor charge formula

$$N = \frac{2\pi r L f \Delta V C_m}{q_e} = \frac{A f \Delta V C_m}{q_e} \tag{1}$$

where r is the radius, L is the length, $A = 2\pi r L$ is the surface area, f is the fraction of unmyelinated active membrane, ΔV is the voltage change, $C_m = 1$ μF/cm^2 is the specific membrane capacitance, and $q_e = 160.218$ zC is the elementary electric charge.

Dendrites are completely unmyelinated $f = 1$. They are depolarized by $\Delta V = 50$ mV during the backpropagation of an action potential (Attwell & Laughlin, 2001). Direct substitution in Eq. (1) establishes that, for each action potential, in the basal dendrites with mean total length $L = 3513$ μm and average radius $r = 0.54$ μm enter $N_{basal} = 3.72 \times 10^7$ Na^+ ions, whereas in apical dendrites with mean total length $L = 5295$ μm and average radius $r = 0.63$ μm enter $N_{apical} = 6.54 \times 10^7$ Na^+ ions.

Axons are heavily myelinated with $f = 0.018$ as estimated from the mean length of unmyelinated nodes

of Ranvier, which is 1.5 μm, and the internode mean distance of 81.7 μm (Arancibia-Cárcamo et al., 2017). During an action potential, axons are depolarized by $\Delta V = 110$ mV (Schwindt et al., 1997). Again, direct substitution in Eq. (1) establishes that, for axonal trees with mean total length $L = 79020$ μm and average radius $r = 0.45$ μm, enter $N_{\text{axon}} = 2.76 \times 10^7$ Na$^+$ ions per action potential.

For a pyramidal soma with surface area $A = 2970 \pm 514$ μm^2 (Zhu, 2000), $f = 1$ and $\Delta V = 110$ mV, direct substitution in Eq. (1) establishes that there is an additional load of $N_{\text{soma}} = 2.04 \times 10^7$ Na$^+$ ions.

For a realistic estimate of the total Na$^+$ entry into a pyramidal neuron per action potential, the amount of Na$^+$ ions computed from the capacitor charge formula should be multiplied by an overlap factor f_{overlap} in order to account for simultaneous activation of Na$^+$ and K$^+$ channels with Hodgkin–Huxley kinetics

$$N_{\text{HH}} = f_{\text{overlap}} \times (N_{\text{basal}} + N_{\text{apical}} + N_{\text{axon}} + N_{\text{soma}}) \tag{2}$$

Computational simulations by Attwell & Laughlin (2001) have found that $f_{\text{overlap}} = 4$. The total sodium load in dendrites, soma and axon obtained from Eq. (2) amounts to $N_{\text{HH}} = 6.024 \times 10^8$ Na$^+$ ions. These Na$^+$ ions need to be pumped out of the neuron by protein Na$^+$/K$^+$-ATPase, which exports 3 Na$^+$ ions and imports 2 K$^+$ ions for every ATP molecule that is consumed (Sengupta et al., 2013). Thus, for each electric spike, to remove the load of Na$^+$ ions each neuron needs $N_{\text{HH}}/3 = 2.008 \times 10^8$ ATP molecules, which amounts to 12.87 pJ of energy (Figure 3b).

2.4.4. Exocytosis of synaptic vesicles

Exocytosis with subsequent endocytosis of a single synaptic vesicle consumes 1.24×10^4 ATP molecules (Attwell & Laughlin, 2001). Recycling of 4000 glutamate neurotransmitter molecules released per vesicle, through glutamate uptake by glial cells, glial conversion to glutamine, export of glutamine to neurons, neuronal conversion to glutamate and re-packaging into synaptic vesicles, consumes another 1.1×10^4 ATP molecules (Attwell & Laughlin, 2001). Thus, the total energy consumption by a single synaptic vesicle is 2.34×10^4 ATP molecules.

Axons of cortical pyramidal neurons form between 7000 and 8000 synapses onto target neurons (Braitenberg & Schüz, 1998). The number of released synaptic vesicles N_{released} is proportional to the total number of axonal synapses N_{synapses} and the probability of release p_{release} of a synaptic vesicle per action potential per synapse

$$N_{\text{released}} = p_{\text{release}} \times N_{\text{synapses}} \tag{3}$$

Considering that the release probability of a synaptic vesicle is only 0.25 per action potential per synapse (Georgiev & Glazebrook, 2018), each pyramidal neuron will release on average 1875 vesicles (for projection neurons most of the targets can be extracortical). Thus, for each electric spike, the exocytosis of synaptic vesicles consumes 4.39×10^7 ATP molecules, which amounts to 2.81 pJ of energy (Figure 3b).

2.4.5. Synaptic activity in dendrites

Action potentials cannot be spontaneously generated by healthy pyramidal neurons from their resting state. Instead, a significant amount of preceding dendritic activity would be required to excite the neuron. An important factor in many related scenarios is the nature and effect of spatial compartmentalization. For instance, Polsky et al. (2004) observed that rat neocortical pyramidal neurons initially process their synaptic inputs within thin dendritic subunits regulated by a nonlinear sigmoidal-type threshold, and then at a second stage they are linearly combined to deliver the overall neuronal response.

Each excitatory synaptic input delivered at a dendrite spine-head depolarizes the soma by only 0.12 mV (Kubota et al., 2015). Thus, for a potential rise of 16 mV, from the resting membrane potential of -70 mV to the spike threshold of -54 mV, summation of at least 134 dendritic spine inputs would be needed. Indeed, based on detailed experimental electrophysiological data *in vivo* using two-photon activation of an intracellular caged NMDA receptor antagonist, it was confirmed that the dendrites of pyramidal neurons need to receive an excess of excitatory synaptic inputs $N_{\text{excess}} = 140$ (activating NMDA and AMPA receptors) in order to trigger an action potential (Palmer et al., 2014).

In the awake state characterized by γ-frequency electric oscillations, the activation of powerful perisomatic inhibition by fast-spiking interneurons (Georgiev et al., 2014; Hu et al., 2014), however, causes

hyperpolarization or shunting that suppresses the effects of excitatory synaptic activation in pyramidal neurons. To take into account the effect of cortical inhibition in the presence of non-zero excitatory to inhibitory (E/I) ratio, the number of dendritic synaptic inputs N_{inputs} can be modeled as

$$N_{\text{inputs}} = N_{\text{excess}} \times \left(1 + \frac{1}{\text{E/I ratio}}\right) \tag{4}$$

The E/I ratio at the soma of layer 2/3 pyramidal neurons is 0.8, whereas at the soma of layer 5 pyramidal neurons it is 0.2 (Yang & Sun, 2018). Direct substitution in Eq. (4) shows that, in the presence of active inhibitory interneurons, the generation of an electric spike would require 315 dendritic inputs for layer 2/3 pyramidal neurons and 840 dendritic inputs for layer 5 pyramidal neurons. For the estimation of the energy budget, we will take the average requirement of 578 excitatory synaptic inputs delivered to the dendritic tree for triggering of an action potential in a single cortical pyramidal neuron.

The release of a single synaptic vesicle filled with glutamate leads to activation of post-synaptic NMDA and AMPA receptors whose opening lets 3.8×10^5 Na^+ ions and 10^4 Ca^{2+} ions enter into the dendrite (Attwell & Laughlin, 2001). Calcium signaling in dendrites leads to Ca^{2+} load that needs to be removed by Na^+/Ca^{2+} exchanger, which exports 1 Ca^{2+} ion and imports 3 Na^+ ions. The 3 Na^+ ions are subsequently exported by Na^+/K^+-ATPase consuming 1 ATP molecule. For 578 synaptic inputs per action potential, the extrusion of the Na^+ and Ca^{2+} ion load requires 7.9×10^7 ATP molecules. Recycling of the vesicles (discussed in the preceding subsection) further requires 1.35×10^7 ATP molecules. The energy expenditure for Ca^{2+} signaling during backpropagation of the action potential from axonal hillock to dendrites adds another 2.61×10^7 ATP molecules (Attwell & Laughlin, 2001). Thus, for each electric spike, dendritic signaling consumes 1.186×10^8 ATP molecules in total, which amounts to 7.60 pJ of energy (Figure 3b).

2.4.6. Rationing of the energy budget across physiological activities

Taking stock of matters so far, we see that neural information is indeed costly. The energy expenses by a single neuron to support the dendritic synaptic activity required to elicit an action potential, to sustain the propagation of the action potential towards pre-synaptic axonal buttons, and to execute the associated release of synaptic vesicles for neurotransmitter signaling, sum up to 3.633×10^8 ATP molecules, which release 23.28 pJ of free energy. For 1.634×10^{10} neurons in the human cerebral cortex (Table 4), the required energy to fire once is 0.38 J. After subtraction from the total cortical budget of the energies spent on the resting membrane potential by neurons and glial cells, there is a remaining energy power of 3.663 W that can be spent by the cerebral cortex on firing action potentials with an average frequency of 9.6 Hz. This constitutes $\approx 14.3\%$ of the maximal firing frequency of 67 Hz that can be attained by layer 5 pyramidal neurons (Schwindt et al., 1997). For average spiking frequency of 9.6 Hz, the duration of the interspike interval is ≈ 104 ms. Thus, for each electric spike, the maintenance of neuronal resting membrane potential in the preceding interspike interval uses 2.28 pJ and the glial support uses 2.59 pJ of energy (Figure 3b).

The total energy budget for a single electric spike together with the preceding interspike interval amounts to 28.15 pJ. In summary, 45.7 % of the energy budget is dedicated for propagation of the action potential, 27.0 % for support of dendritic synaptic activity, 10.0 % for exocytosis of synaptic vesicles, 9.2 % for glial support, and 8.1 % for maintenance of the neuronal resting membrane potential in the interspike interval (Figure 3c).

Original estimates by Attwell & Laughlin (2001) pointed to 3.29×10^9 ATP molecules (210.85 pJ) consumed by a neuron with a mean firing rate of 4 Hz. The energy budget stipulated 47% for the production of action potentials, 34% for the activity of dendritic post-synaptic receptors, 6% for presynaptic exocytosis including recycling of excess glutamate, and 13% for maintenance of the resting state of neurons and supporting glial cells. The main difference between that previous study and our present results stems from the precise morphometric data that we have used resulting in higher average spiking frequency by pyramidal neurons due to lower energy needs to support action potentials.

2.4.7. The Landauer limit

Moving a single elementary electric charge (electron, proton or monovalent ion) across the plasma membrane through a potential difference of 110 mV dissipates 0.11 eV of energy. The energy of 23.28 pJ consumed

per action potential is sufficient for the motion of 1.32×10^9 elementary electric charges. The transport of an elementary electric charge across the plasma membrane, however, may not be the elementary bit of neuronal logical operation. Landauer's limit asserts that the minimum possible amount of energy required by thermodynamics to erase one bit of information (e.g. through application of an irreversible gate such as AND gate or OR gate) is

$$E_{\min} = k_B T \ln 2 \tag{5}$$

recalling that $k_B = 1.38 \times 10^{-23}$ J/K is Boltzmann's constant and T is the absolute temperature (Landauer, 1961). Otherwise expressed, if ΔE_{env} denotes energy dissipated into the environment, and ΔS_{sys} the thermodynamic entropy equivalent to information erased from the system memory, then

$$\Delta E_{\mathrm{env}} \geq T \Delta S_{\mathrm{sys}} \tag{6}$$

The total number of erased bits of information I_{erased} from the system is bounded by (Bormashenko, 2019; Street, 2020)

$$I_{\mathrm{erased}} \leq \frac{\Delta E_{\mathrm{env}}}{k_B T \ln 2} \tag{7}$$

At physiological temperature of 310 K, Landauer's limit is 2.968 zJ (18.526 meV). Therefore, the energy of 23.28 pJ consumed per action potential is sufficient for the execution of 7.844×10^9 Landauer elementary logical operations. Noteworthy, the passage of a single elementary electric charge across the plasma membrane is equivalent to ≈ 5.94 such elementary logical operations. Since each S4 protein α-helix voltage-sensor in voltage-gated ion channels (Figure 4) usually contains 6 positively charged amino acid residues (Catterall, 1988), the proton tunneling between neighboring positively charged sites in the S4 voltage-sensor (Kariev & Green, 2012, 2018, 2019; Kariev et al., 2007) is ideally suited to represent a single Landauer elementary logical operation in cortical neural networks. Protons interact with water and biological matter, mainly in a non-classical manner including exchange-correlation effects, chemical bonding in hydronium-like complexes, and tunneling (Lobaugh & Voth, 1996). Once the S4 protein α-helix voltage-sensors adopt an open channel conformation, the subsequent flow of metal ions across the ion channel leads to amplification of individual events of proton quantum tunneling that occurred in the S4 voltage sensors (Kariev & Green, 2012, 2018, 2019; Kariev et al., 2007). This is how nanoscale quantum events may be amplified to exert macroscopic effect on neuronal behavior and brain function (Georgiev, 2013, 2020). If the energy power of 3.663 W available for electric spiking is completely miniaturized at the Landauer limit of 2.968 zJ, the human brain cortex will be able to execute the equivalent of over 1.2 zetta elementary logical operations per second.

3. Discussion

In this work, we have evaluated the cognitive computational capacity of the brain based on its experimentally measured glucose consumption (Herculano-Houzel, 2011). The tightness of the bound is justified by two biomedical facts. Firstly, the brain does not have an internal store of glucose, but needs to rely on blood glucose level maintained by physiologically regulated release from the liver glycogen depot (Guyton & Hall, 2006). Secondly, the brain does not have anything like a long-term energy battery capable of supporting cognitive computation in the absence of glucose, because loss of clinical consciousness (syncope) occurs within seconds of a sudden drop in blood glucose levels, or a brief cessation of cerebral blood flow (Kapoor, 2000). This implies that the rate of glucose consumption indeed puts a tight upper bound on the brain's capacity for cognitive computation.

In the awake state, the energy power of 4.427 W consumed by the human cerebral cortex permits a maximal average spiking rate of 9.6 Hz. This is consistent with the observed average spontaneous firing rate of 12.87 Hz by neurons in the visual cortex of awake rhesus monkeys (Chen et al., 2009), albeit it is somewhat higher than the average spontaneous firing rates of 3.28 Hz in rat (Aasebø et al., 2017) or 1.88 Hz in mouse (Durand et al., 2016). Evoked activity of neurons in primary visual cortex of awake mice in response to an optimal drifting grating, however, exhibited average firing rates that were strongly dependent on locomotion: 2.9 Hz for stationary mice and 8.2 Hz for mice running on a freely rotating
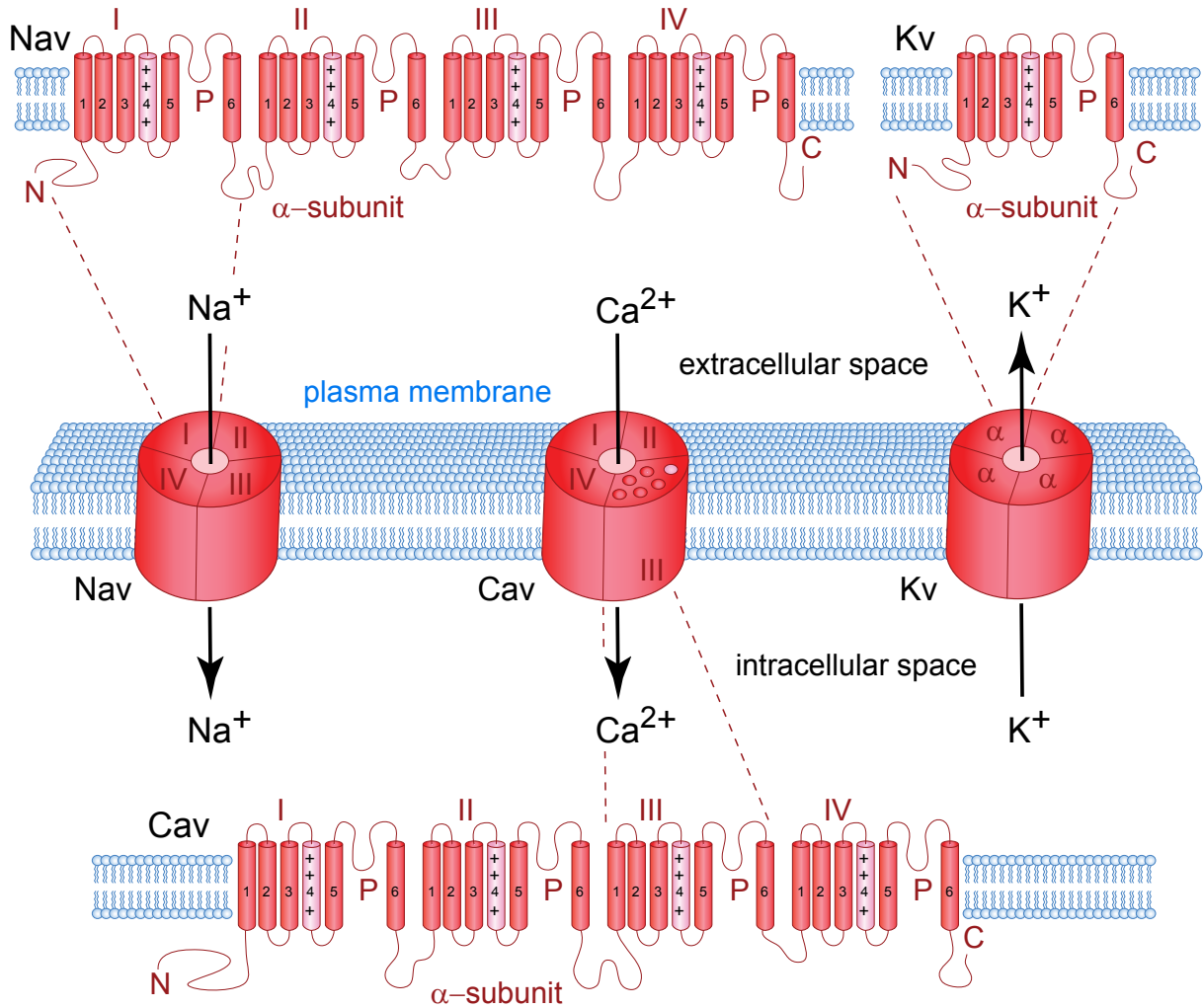
10

Figure 4: Electric activities of pyramidal neurons are generated by sodium (Nav), potassium (Kv) and calcium (Cav) voltage-gated ion channels incorporated into the plasma membrane, which consists of a phospholipid bilayer with thickness of 10 nanometers. Structurally, individual voltage-gated ion channels contain four protein domains I-IV. Each domain has six transmembrane α-helices (1-6). The pore of the ion channel is configured by protein loops (P) connecting the 5th and 6th α-helices. Voltage sensing is accomplished by the 4th α-helix (S4), which usually carries six positively charged lysine or arginine amino acid residues. Each proton tunneling event between neighboring positively charged sites in the S4 voltage-sensor is ideally suited to represent a single Landauer elementary logical operation.

spherical treadmill with their heads fixed (Niell & Stryker, 2010). Thus, the estimated maximal average spiking rate of 9.6 Hz might be reached by an active brain engaged in a complex problem-solving task that integrates multi-modal information from different senses.

Detailed analysis of neuronal morphology combined with energetics of electrophysiological and molecular processes support the highly efficient miniaturization of logical computational gates performed by pyramidal neurons in the cerebral cortex. The energy utilized for the generation of a single action potential is sufficient for the execution of 7.844×10^9 elementary logical operations. The cerebral cortex appears to have attained the maximal computational efficiency allowed by Landauer's thermodynamic limit: quantum tunneling of a proton between neighboring positively charged S4 sensor sites in voltage-gated ion channels constitutes a single Landauer elementary logical operation, whereas the transport of a monovalent metal ion through the open ion channel pore constitutes six such operations.

Landauer's limit sets ultimate energy constrains on the functioning of physical computing devices in the presence of a thermal bath (Gaudenzi et al., 2018; Hong et al., 2016; Lent et al., 2019; Sagawa & Ueda, 2008, 2010). The original formulation put forward by Landauer (1961) is motivated by consideration of the finite capacity of working memory of computing devices, namely the act of resetting of the working memory to its initial empty state requires compression of the phase space of the memory device, which will decrease its entropy. The second law of thermodynamics, however, requires that the total entropy of the memory device and its environment increases in time (Leff & Rex, 2002). Therefore, resetting the working memory must be accompanied by a corresponding entropy increase in the environment, in the form of heat dissipation, which is at least $k_B T \ln 2$ joules per bit (Landauer, 1961). The brain cortex, which is responsible for the stream of consciousness, allows us to store cognitive information only for short time periods before we forget it, or replace it with new sensory information. Thus, one interpretation of Landauer's principle is that the working of the human mind spends energy to forget (Plenio & Vitelli, 2001), where the energy dissipation occurs in the act of irreversible resetting of the cortical working memory. An alternative formulation based on the theory of dissipative quantum channels, however, establishes that communication of classical information across a noisy quantum channel (Jagadish & Petruccione, 2018) that is immersed in a heat bath with effective temperature T, also requires energy expenditure of at least $k_B T \ln 2$ joules per bit (Levitin, 1998; Porod et al., 1984). Otherwise, the signal transmitted from the sender gate to the receiver gate could not be distinguished from the ambient thermal noise (Levitin, 1998; Porod et al., 1984). Thus, another interpretation of Landauer's principle is that the working of the human mind spends energy to transmit information between different noisy neuronal compartments (dendrites, soma, axon) or to communicate unambiguously with effector organs (e.g. muscles through intermediate extracortical centers such as α-motor neurons in the spinal cord). It is likely that, in the course of an electric spike, cortical pyramidal neurons spend energy both for resetting their S4 voltage sensors in the resting ion channel state and for transmission of the electric signal from dendrites toward the axon terminals. Much related are implications of this neurophysiology together with Landauer's principle for human cognition, as discussed in Collel & Fauquet (2015); Street (2016, 2020) with significant pointers towards variational free energy and its role in perceptual Bayesian inference (Friston, 2010, 2013).

Because physical dynamics at the nanoscale is able to manifest characteristic quantum mechanical effects, our results provide a rigorous foundation, as far as energy considerations are concerned, for future development of quantum models of the transmembrane electromagnetic field and its interaction with mobile electric charges inside protein voltage-gated ion channels (Georgiev, 2017; Kariev & Green, 2012, 2018, 2019; Kariev et al., 2007) or membrane-bound SNARE proteins whose zipping mechanism triggers neurotransmitter release (Georgiev & Glazebrook, 2018, 2019a,b). Technological advances in available supercomputers have already led to routine simulation of quantum dynamics of small biomolecules in electrolyte solution with the use of quantum chemistry software implementing density functional theory (Kolev et al., 2013, 2018, 2011). Applications of recent theorems in quantum information, as based on generalized uncertainty relations (Carmi & Cohen, 2019) to quantum brain states (Georgiev, 2013, 2020) may further shed light on the perplexing open problems in the cognitive sciences.

To summarize, we have implemented fundamental physical principles, including the thermodynamically allowable Landauer's limit of energy spent on elementary logical operations, to show that not all biomolecular processes may contribute to cognitive computation, but mainly those involving transmembrane proteins, such as voltage-gated or ligand-gated ion channels, integrated into the electrically excitable neuronal plasma membrane. Even though the human cerebral cortex may perform over 1.2 zetta logical operations per second, exceeding over four orders of magnitude the capacity of modern supercomputers, we expect the implementation of large-scale and ultra in-depth brain simulations to significantly advance in the foreseeable future.

4. Conflict of Interest

5. Methods and Materials

5.1. Selection criteria for the morphometric study

Morphometric parameters such as radii and lengths of neuronal projections constrain the electric performance of neurons and determine the number of physical charges that need to cross the plasma membrane in order to elicit a certain change in the transmembrane voltage. For accurate assessment of the average radii and total lengths of different neurites (basal dendrites, apical dendrites, and axons), we have analyzed the full collection of pyramidal neuronal reconstructions in rodent (mouse, rat) or human brain cortex from NeuroMorpho.org 7.8 digital archive (Ascoli et al., 2007) that pass the following selection criteria: Firstly, we have selected only control experimental conditions with animals that did not express genetically-engineered disease-related protein mutations and were not exposed to pharmacological agents or harmful stimuli (e.g. stress). Secondly, only animals whose age corresponds to human age of over 3 months old were included. The utilized piecewise linear conversion formulas into corresponding human age are given for mice by Sengupta (2013), and for rats by Dutta & Sengupta (2016). Thirdly, to ensure minimal trimming of dendritic trees for analysis of apical and basal dendrites, we have included only reconstructions with minimal slice thickness of 300 μm. Analysis of complete axonal arborizations was performed in neuronal reconstructions from brain-wide imaging data (Economo et al., 2016; Gerfen et al., 2018). To verify the quality of all reconstructions, neurons were visualized in Neuromantic version 1.6.3 (https://www.reading.ac.uk/neuromantic/body_index.php) and .swc files with non-standard labeling of neurites or visually incomplete dendritic tree (e.g. apical dendrite was trimmed near its base) were excluded from further analysis. Standardized .swc files are tables with 7 columns of numerical data for cable-like cylindrical segments that comprise the neuronal reconstruction (Table 6). The lengths and volumes of neurite segments was quantified with the use of custom Excel macros fetching the cable radii and computing the Euclidean distances from the x, y, z coordinates given in the .swc files. Morphometric data are reported as mean ± standard deviation.

Table 6: Table structure of standardized .swc files.

1	2	3	4	5	6	7
segment number	structure identifier	x position	y position	z position	radius r	parent segment
integer value starting from 1	1 - soma 2 - axon 3 - basal dendrite 4 - apical dendrite	coordinate in μm	coordinate in μm	coordinate in μm	segment radius in μm	parent segment number; -1 is used for lack of parent

5.2. Neuronal reconstructions

Digital reconstructions of pyramidal neurons in control experimental conditions were selected from three animal species: mouse (252 neurons), rat (491 neurons) and human (6 neurons). This dataset of 749 neurons includes contributions from 32 labs: Amaral (Ishizuka et al., 1995), Arnold_Johnston (Arnold et al., 2019), Barrionuevo (Henze et al., 1996), Blackman (Blackman et al., 2014), Buchs (Larkum et al., 2004), Chandrashekar (Economo et al., 2016), Claiborne (Carnevale et al., 1997), De Koninck (Bories et al., 2013), Dendritica (Vetter et al., 2001), Feldmeyer (Marx & Feldmeyer, 2012; Marx et al., 2015), Groen (Groen et al., 2014), Hay (Hay et al., 2013), Helmstaedter (Helmstaedter et al., 2008), Hoffman (Hoffmann et al., 2015), Jaffe (Chitwood et al., 1999), Johnston (Dougherty et al., 2012; Malik et al., 2016), Kawaguchi (Hirai et al., 2012; Ueta et al., 2013), Kole (Hallermann et al., 2012; Hamada et al., 2016; Hamada & Kole, 2015; Kole, 2011; Kole et al., 2007, 2004), Korngreen (Bar-Yehuda & Korngreen, 2008), Krieger (Groh et al., 2009; Krieger et al., 2007), Luo (Gong et al., 2016), Markram (Anastassiou et al., 2015), Martina (Kelly et al., 2016), MouseLight (Gerfen et al., 2018), Orion (Santamaría-Pang et al., 2015), Segev (Eyal et al., 2016), Soltesz (Lee et al., 2014), Spruston (Golding et al., 2005), Staiger (Staiger et al., 2016), Storm (Hönigsperger et al., 2015), Topolnik (Francavilla et al., 2018; Tyan et al., 2014) and Urban (Tripathy et al., 2015; Zhou et al., 2015).

13

5.3. Modeling of cortical layers

Vector .svg images of individual neurons were rendered with HBP Neuron Morphology Viewer (Bakker et al., 2017; Bakker & Tiesinga, 2016) and scaling information was extracted with NeuroM, a Python-based toolkit for the analysis and processing of neuron morphologies developed by the Blue Brain Project (https://neurom.readthedocs.io/en/stable/). Modeling of the brain cortex in mouse was then performed in Adobe Illustrator based on measured thickness of cortical layers in Nissl stained coronal slices (Franklin & Paxinos, 2007; Georgiev et al., 2016). All data from NeuroMorpho.Org digital archive was used in compliance with the online Terms of Use (http://neuromorpho.org/useterm.jsp). In particular, all original papers that describe the reconstructions are cited, the complete name of the digital archive is clearly stated, attribution to the developers of the archive is given (Ascoli et al., 2007), and specific reconstructions are referenced with their NeuroMorpho.Org ID numbers.

5.4. Statistical analysis

Statistical analysis of neuronal morphology was performed using SPSS ver. 23 (IBM Corporation, New York, USA). Comparison of morphometric measures for apical and basal dendrites was performed with repeated-measures analysis of variance (rANOVA) implemented as a general linear model in which within-subject variable was dendrite type, between-subject factors were animal species, brain region and neuronal type, and covariate was slice thickness. Comparison of axons with dendrites was performed with paired t-tests for a subset of the neuronal reconstructions for which the axonal trees were complete. Paired box plots were created with the use of ggpubr library in R ver. 4.0.2 (R Foundation for Statistical Computing, Vienna, Austria, https://www.r-project.org/).

5.5. Energy consumption and energy units

The energy consumption by pyramidal neurons in different animal species (mouse, rat or humans) was estimated based on brain mass, glucose use per gram per minute, and total number of neurons in the brain or the cerebral cortex reported in Herculano-Houzel (2011). For each molecule of glucose, oxidative metabolism in mitochondria produces 32 ATP molecules (Mergenthaler et al., 2013). Hydrolysis of 1 ATP molecule releases 0.4 eV of free energy (George et al., 1970; Scott, 2005), which is equivalent to 64.0872 zJ. Thus, the useable energy from 1 glucose molecule is 12.8 eV (2050.79 zJ). For molecular processes the energy consumption was reported in electron volts (eV), where 1 eV is the amount of energy required to move 1 electron across an electric potential difference of 1 V. For macroscopic processes the energy consumption was reported in joules (J), using a conversion formula where 1 eV equals to 160.218 zJ. Brain power was reported in watts (W), where 1 W is defined to be the energy transfer at a rate of 1 J per second. For all reported quantities standard SI prefixes were used.

References

Aasebø, I. E. J., Lepperød, M. E., Stavrinou, M., Nøkkevangen, S., Einevoll, G., Hafting, T., & Fyhn, M. (2017). Temporal processing in the visual cortex of the awake and anesthetized rat. *eNeuro*, *4*, eneuro.0059–17.2017. doi:10.1523/eneuro.0059-17.2017.

Anastassiou, C. A., Perin, R., Buzsáki, G., Markram, H., & Koch, C. (2015). Cell type- and activity-dependent extracellular correlates of intracellular spiking. *Journal of Neurophysiology*, *114*, 608–623. doi:10.1152/jn.00628.2014.

Arancibia-Cárcamo, I. L., Ford, M. C., Cossell, L., Ishida, K., Tohyama, K., & Attwell, D. (2017). Node of Ranvier length as a potential regulator of myelinated axon conduction speed. *eLife*, *6*, e23329. doi:10.7554/eLife.23329.

Arnold, E. C., McMurray, C., Gray, R., & Johnston, D. (2019). Epilepsy-induced reduction in HCN channel expression contributes to an increased excitability in dorsal, but not ventral, hippocampal CA1 neurons. *eNeuro*, *6*, eneuro.0036–19.2019. doi:10.1523/eneuro.0036-19.2019.

Ascoli, G. A., Donohue, D. E., & Halavi, M. (2007). NeuroMorpho.org: a central resource for neuronal morphologies. *Journal of Neuroscience*, *27*, 9247–9251. doi:10.1523/jneurosci.2055-07.2007.

Attwell, D., & Laughlin, S. B. (2001). An energy budget for signaling in the grey matter of the brain. *Journal of Cerebral Blood Flow and Metabolism*, *21*, 1133–1145. doi:10.1097/00004647-200110000-00001.

Azevedo, F. A. C., Carvalho, L. R. B., Grinberg, L. T., Farfel, J. M., Ferretti, R. E. L., Leite, R. E. P., Filho, W. J., Lent, R., & Herculano-Houzel, S. (2009). Equal numbers of neuronal and nonneuronal cells make the human brain an isometrically scaled-up primate brain. *Journal of Comparative Neurology*, *513*, 532–541. doi:10.1002/cne.21974.

Bakker, R., García-Amado, M., Evangelio, M., Clascá, F., & Tiesinga, P. H. (2017). Workflow, data format and tools to register neuron morphologies to a reference brain atlas. *BMC Neuroscience*, *18*, P271. doi:10.1186/s12868-017-0372-1.

Bakker, R., & Tiesinga, P. H. (2016). Web-based neuron morphology viewer as an aid to develop new standards for neuron morphology file formats. *Frontiers in Neuroinformatics*, . doi:10.3389/conf.fninf.2016.20.00079.

Bar-Yehuda, D., & Korngreen, A. (2008). Space-clamp problems when voltage clamping neurons expressing voltage-gated conductances. *Journal of Neurophysiology*, *99*, 1127–1136. doi:10.1152/jn.01232.2007.

Bekkers, J. M. (2011). Pyramidal neurons. *Current Biology*, *21*, R975. doi:10.1016/j.cub.2011.10.037.

Blackman, A. V., Grabuschnig, S., Legenstein, R., & Sjöström, P. J. (2014). A comparison of manual neuronal reconstruction from biocytin histology or 2-photon imaging: morphometry and computer modeling. *Frontiers in Neuroanatomy*, *8*, 65. doi:10.3389/fnana.2014.00065.

Bories, C., Husson, Z., Guitton, M. J., & De Koninck, Y. (2013). Differential balance of prefrontal synaptic activity in successful versus unsuccessful cognitive aging. *Journal of Neuroscience*, *33*, 1344. doi:10.1523/jneurosci.3258-12.2013.

Bormashenko, E. (2019). The Landauer principle: re-formulation of the second thermodynamics law or a step to great unification? *Entropy*, *21*, 918. doi:10.3390/e21100918.

Braitenberg, V., & Schüz, A. (1998). *Cortex: Statistics and Geometry of Neuronal Connectivity*. (2nd ed.). Berlin: Springer. doi:10.1007/978-3-662-03733-1.

Carmi, A., & Cohen, E. (2019). Relativistic independence bounds nonlocality. *Science Advances*, *5*, eaav8370. doi:10.1126/sciadv.aav8370.

Carnevale, N. T., Tsai, K. Y., Claiborne, B. J., & Brown, T. H. (1997). Comparative electrotonic analysis of three classes of rat hippocampal neurons. *Journal of Neurophysiology*, *78*, 703–720. doi:10.1152/jn.1997.78.2.703.

Catterall, W. A. (1988). Structure and function of voltage-sensitive ion channels. *Science*, *242*, 50. doi:10.1126/science.2459775.

Chen, Y., Anand, S., Martinez-Conde, S., Macknik, S. L., Bereshpolova, Y., Swadlow, H. A., & Alonso, J.-M. (2009). The linearity and selectivity of neuronal responses in awake visual cortex. *Journal of Vision*, *9*, 12–12. doi:10.1167/9.9.12.

Chitwood, R. A., Hubbard, A., & Jaffe, D. B. (1999). Passive electrotonic properties of rat hippocampal CA3 interneurones. *Journal of Physiology*, *515*, 743–756. doi:10.1111/j.1469-7793.1999.743ab.x.

Collel, G., & Fauquet, J. (2015). Brain activty and cognition: a connection from thermodynamics and information theory. *Frontiers in Psychology*, *6*. doi:10.3389/fpsyg.2015.00818.

Dougherty, K. A., Islam, T., & Johnston, D. (2012). Intrinsic excitability of CA1 pyramidal neurones from the rat dorsal and ventral hippocampus. *Journal of Physiology*, *590*, 5707–5722. doi:10.1113/jphysiol.2012.242693.

Durand, S., Iyer, R., Mizuseki, K., de Vries, S., Mihalas, S., & Reid, R. C. (2016). A comparison of visual response properties in the lateral geniculate nucleus and primary visual cortex of awake and anesthetized mice. *Journal of Neuroscience*, *36*, 12144–12156. doi:10.1523/jneurosci.1741-16.2016.

Dutta, S., & Sengupta, P. (2016). Men and mice: relating their ages. *Life Sciences*, *152*, 244–248. doi:10.1016/j.lfs.2015.10.025.

Economo, M. N., Clack, N. G., Lavis, L. D., Gerfen, C. R., Svoboda, K., Myers, E. W., & Chandrashekar, J. (2016). A platform for brain-wide imaging and reconstruction of individual neurons. *eLife*, *5*, e10566. doi:10.7554/eLife.10566.

Eyal, G., Verhoog, M. B., Testa-Silva, G., Deitcher, Y., Benavides-Piccione, R., DeFelipe, J., de Kock, C. P. J., Mansvelder, H. D., & Segev, I. (2018). Human cortical pyramidal neurons: from spines to spikes via models. *Frontiers in Cellular Neuroscience*, *12*, 181. doi:10.3389/fncel.2018.00181.

Eyal, G., Verhoog, M. B., Testa-Silva, G., Deitcher, Y., Lodder, J. C., Benavides-Piccione, R., Morales, J., DeFelipe, J., de Kock, C. P. J., Mansvelder, H. D., & Segev, I. (2016). Unique membrane properties and enhanced signal processing in human neocortical neurons. *eLife*, *5*, e16553. doi:10.7554/eLife.16553.

Fournier, J., Müller, C. M., & Laurent, G. (2015). Looking for the roots of cortical sensory computation in three-layered cortices. *Current Opinion in Neurobiology*, *31*, 119–126. doi:10.1016/j.conb.2014.09.006.

Francavilla, R., Villette, V., Luo, X., Chamberland, S., Muñoz Pino, E., Camiré, O., Wagner, K., Kis, V., Somogyi, P., & Topolnik, L. (2018). Connectivity and network state-dependent recruitment of long-range VIP-GABAergic neurons in the mouse hippocampus. *Nature Communications*, *9*, 5043. doi:10.1038/s41467-018-07162-5.

Franklin, K. B. J., & Paxinos, G. (2007). *The Mouse Brain in Stereotaxic Coordinates*. Amsterdam: Academic Press.

Friston, K. J. (2010). The free-energy principle: A unified brain theory? *Nature Reviews Neuroscience*, *11*, 127–138.

Friston, K. J. (2013). Life as we know it. *Journal of The Royal Society Interface*, *10*, 20130475.

Gaudenzi, R., Burzurí, E., Maegawa, S., van der Zant, H. S. J., & Luis, F. (2018). Quantum Landauer erasure with a molecular nanomagnet. *Nature Physics*, *14*, 565–568. doi:10.1038/s41567-018-0070-7.

George, P., Witonsky, R. J., Trachtman, M., Wu, C., Dorwart, W., Richman, L., Richman, W., Shurayh, F., & Lentz, B. (1970). "Squiggle-H_2O". An enquiry into the importance of solvation effects in phosphate ester and anhydride reactions. *Biochimica et Biophysica Acta (BBA) - Bioenergetics*, *223*, 1–15. doi:10.1016/0005-2728(70)90126-X.

Georgiev, D., Arion, D., Enwright, J. F., Kikuchi, M., Minabe, Y., Corradi, J. P., Lewis, D. A., & Hashimoto, T. (2014). Lower gene expression for KCNS3 potassium channel subunit in parvalbumin-containing neurons in the prefrontal cortex in

15

schizophrenia. *American Journal of Psychiatry*, *171*, 62–71. doi:10.1176/appi.ajp.2013.13040468.

Georgiev, D., Yoshihara, T., Kawabata, R., Matsubara, T., Tsubomoto, M., Minabe, Y., Lewis, D. A., & Hashimoto, T. (2016). Cortical gene expression after a conditional knockout of 67 kDa glutamic acid decarboxylase in parvalbumin neurons. *Schizophrenia Bulletin*, *42*, 992–1002. doi:10.1093/schbul/sbw022.

Georgiev, D. D. (2013). Quantum no-go theorems and consciousness. *Axiomathes*, *23*, 683–695. doi:10.1007/s10516-012-9204-1.

Georgiev, D. D. (2017). *Quantum Information and Consciousness: A Gentle Introduction*. Boca Raton: CRC Press. doi:10.1201/9780203732519.

Georgiev, D. D. (2020). Inner privacy of conscious experiences and quantum information. *Biosystems*, *187*, 104051. doi:10.1016/j.biosystems.2019.104051.

Georgiev, D. D., & Glazebrook, J. F. (2018). The quantum physics of synaptic communication via the SNARE protein complex. *Progress in Biophysics and Molecular Biology*, *135*, 16–29. doi:10.1016/j.pbiomolbio.2018.01.006.

Georgiev, D. D., & Glazebrook, J. F. (2019a). On the quantum dynamics of Davydov solitons in protein α-helices. *Physica A: Statistical Mechanics and its Applications*, *517*, 257–269. doi:10.1016/j.physa.2018.11.026.

Georgiev, D. D., & Glazebrook, J. F. (2019b). Quantum tunneling of Davydov solitons through massive barriers. *Chaos, Solitons and Fractals*, *123*, 275–293. doi:10.1016/j.chaos.2019.04.013.

Gerfen, C. R., Economo, M. N., & Chandrashekar, J. (2018). Long distance projections of cortical pyramidal neurons. *Journal of Neuroscience Research*, *96*, 1467–1475. doi:10.1002/jnr.23978.

Golding, N. L., Mickus, T. J., Katz, Y., Kath, W. L., & Spruston, N. (2005). Factors mediating powerful voltage attenuation along CA1 pyramidal neuron dendrites. *Journal of Physiology*, *568*, 69–82. doi:10.1113/jphysiol.2005.086793.

Goldman-Rakic, P. S. (2002). The "psychic cell" of Ramón y Cajal. *Progress in Brain Research*, *136*, 427–434.

Gong, H., Xu, D., Yuan, J., Li, X., Guo, C., Peng, J., Li, Y., Schwarz, L. A., Li, A., Hu, B., Xiong, B., Sun, Q., Zhang, Y., Liu, J., Zhong, Q., Xu, T., Zeng, S., & Luo, Q. (2016). High-throughput dual-colour precision imaging for brain-wide connectome with cytoarchitectonic landmarks at the cellular level. *Nature Communications*, *7*, 12142. doi:10.1038/ncomms12142.

Groen, M. R., Paulsen, O., Pérez-Garci, E., Nevian, T., Wortel, J., Dekker, M. P., Mansvelder, H. D., van Ooyen, A., & Meredith, R. M. (2014). Development of dendritic tonic GABAergic inhibition regulates excitability and plasticity in CA1 pyramidal neurons. *Journal of Neurophysiology*, *112*, 287–299. doi:10.1152/jn.00066.2014.

Groh, A., Meyer, H. S., Schmidt, E. F., Heintz, N., Sakmann, B., & Krieger, P. (2009). Cell-type specific properties of pyramidal neurons in neocortex underlying a layout that is modifiable depending on the cortical area. *Cerebral Cortex*, *20*, 826–836. doi:10.1093/cercor/bhp152.

Guyton, A. C., & Hall, J. E. (2006). *Textbook of Medical Physiology*. (11th ed.). Philadelphia: Elsevier.

Hallermann, S., de Kock, C. P. J., Stuart, G. J., & Kole, M. H. P. (2012). State and location dependence of action potential metabolic cost in cortical pyramidal neurons. *Nature Neuroscience*, *15*, 1007–1014. doi:10.1038/nn.3132.

Hamada, M. S., Goethals, S., de Vries, S. I., Brette, R., & Kole, M. H. P. (2016). Covariation of axon initial segment location and dendritic tree normalizes the somatic action potential. *Proceedings of the National Academy of Sciences*, *113*, 14841. doi:10.1073/pnas.1607548113.

Hamada, M. S., & Kole, M. H. P. (2015). Myelin loss and axonal ion channel adaptations associated with gray matter neuronal hyperexcitability. *Journal of Neuroscience*, *35*, 7272. doi:10.1523/jneurosci.4747-14.2015.

Hay, E., Schürmann, F., Markram, H., & Segev, I. (2013). Preserving axosomatic spiking features despite diverse dendritic morphology. *Journal of Neurophysiology*, *109*, 2972–2981. doi:10.1152/jn.00048.2013.

Helmstaedter, M., Sakmann, B., & Feldmeyer, D. (2008). The relation between dendritic geometry, electrical excitability, and axonal projections of L2/3 interneurons in rat barrel cortex. *Cerebral Cortex*, *19*, 938–950. doi:10.1093/cercor/bhn138.

Henze, D. A., Cameron, W. E., & Barrionuevo, G. (1996). Dendritic morphology and its effects on the amplitude and rise-time of synaptic signals in hippocampal CA3 pyramidal cells. *Journal of Comparative Neurology*, *369*, 331–334. doi:10.1002/(SICI)1096-9861(19960603)369:3<331::AID-CNE1>3.0.CO;2-6.

Herculano-Houzel, S. (2011). Scaling of brain metabolism with a fixed energy budget per neuron: implications for neuronal activity, plasticity and evolution. *PLoS One*, *6*, e17514. doi:10.1371/journal.pone.0017514.

Hirai, Y., Morishima, M., Karube, F., & Kawaguchi, Y. (2012). Specialized cortical subnetworks differentially connect frontal cortex to parahippocampal areas. *Journal of Neuroscience*, *32*, 1898–1913. doi:10.1523/jneurosci.2810-11.2012.

Hoffmann, J. H. O., Meyer, H. S., Schmitt, A. C., Straehle, J., Weitbrecht, T., Sakmann, B., & Helmstaedter, M. (2015). Synaptic conductance estimates of the connection between local inhibitor interneurons and pyramidal neurons in layer 2/3 of a cortical column. *Cerebral Cortex*, *25*, 4415–4429. doi:10.1093/cercor/bhv039.

Hong, J., Lambson, B., Dhuey, S., & Bokor, J. (2016). Experimental test of Landauer's principle in single-bit operations on nanomagnetic memory bits. *Science Advances*, *2*, e1501492. doi:10.1126/sciadv.1501492.

Hönigsperger, C., Marosi, M., Murphy, R., & Storm, J. F. (2015). Dorsoventral differences in Kv7/M-current and its impact on resonance, temporal summation and excitability in rat hippocampal pyramidal cells. *Journal of Physiology*, *593*, 1551–1580. doi:10.1113/jphysiol.2014.280826.

Hu, H., Gan, J., & Jonas, P. (2014). Fast-spiking, parvalbumin+ GABAergic interneurons: from cellular design to microcircuit function. *Science*, *345*, 1255263. doi:10.1126/science.1255263.

Ishizuka, N., Cowan, W. M., & Amaral, D. G. (1995). A quantitative analysis of the dendritic organization of pyramidal cells in the rat hippocampus. *Journal of Comparative Neurology*, *362*, 17–45. doi:10.1002/cne.903620103.

Jagadish, V., & Petruccione, F. (2018). An invitation to quantum channels. *Quanta*, *7*, 54–67. doi:10.12743/quanta.v7i1.77.

Kapoor, W. N. (2000). Syncope. *New England Journal of Medicine*, *343*, 1856–1862. doi:10.1056/nejm200012213432507.

Kariev, A. M., & Green, M. E. (2012). Voltage gated ion channel function: gating, conduction, and the role of water and protons. *International Journal of Molecular Sciences*, *13*, 1680–1709. doi:10.3390/ijms13021680.

Kariev, A. M., & Green, M. E. (2018). The role of proton transport in gating current in a voltage gated ion channel, as shown by quantum calculations. *Sensors*, *18*, 3143. doi:10.3390/s18093143.

Kariev, A. M., & Green, M. E. (2019). Quantum calculation of proton and other charge transfer steps in voltage sensing in the Kv1.2 channel. *Journal of Physical Chemistry B*, *123*, 7984–7998. doi:10.1021/acs.jpcb.9b05448.

Kariev, A. M., Znamenskiy, V. S., & Green, M. E. (2007). Quantum mechanical calculations of charge effects on gating the KcsA channel. *Biochimica et Biophysica Acta (BBA) - Biomembranes*, *1768*, 1218–1229. doi:10.1016/j.bbamem.2007.01.021.

Kelly, C. J., Huang, M., Meltzer, H., & Martina, M. (2016). Reduced glutamatergic currents and dendritic branching of layer 5 pyramidal cells contribute to medial prefrontal cortex deactivation in a rat model of neuropathic pain. *Frontiers in Cellular Neuroscience*, *10*, 133. doi:10.3389/fncel.2016.00133.

Kole, M. H. P. (2011). First node of Ranvier facilitates high-frequency burst encoding. *Neuron*, *71*, 671–682. doi:10.1016/j.neuron.2011.06.024.

Kole, M. H. P., Bräuer, A. U., & Stuart, G. J. (2007). Inherited cortical HCN1 channel loss amplifies dendritic calcium electrogenesis and burst firing in a rat absence epilepsy model. *Journal of Physiology*, *578*, 507–525. doi:10.1113/jphysiol.2006.122028.

Kole, M. H. P., Costoli, T., Koolhaas, J. M., & Fuchs, E. (2004). Bidirectional shift in the cornu ammonis 3 pyramidal dendritic organization following brief stress. *Neuroscience*, *125*, 337–347. doi:10.1016/j.neuroscience.2004.02.014.

Kolev, S. K., Petkov, P. S., Rangelov, M., & Vayssilov, G. N. (2013). Ab initio molecular dynamics of Na^+ and Mg^{2+} countercations at the backbone of RNA in water solution. *ACS Chemical Biology*, *8*, 1576–1589. doi:10.1021/cb300463h.

Kolev, S. K., Petkov, P. S., Rangelov, M. A., Trifonov, D. V., Milenov, T. I., & Vayssilov, G. N. (2018). Interaction of Na^+, K^+, Mg^{2+} and Ca^{2+} counter cations with RNA. *Metallomics*, *10*, 659–678. doi:10.1039/c8mt00043c.

Kolev, S. K., Petkov, P. S., Rangelov, M. A., & Vayssilov, G. N. (2011). Density functional study of hydrogen bond formation between methanol and organic molecules containing Cl, F, NH_2, OH, and COOH functional groups. *Journal of Physical Chemistry A*, *115*, 14054–14068. doi:10.1021/jp204503f.

Krieger, P., Kuner, T., & Sakmann, B. (2007). Synaptic connections between layer 5b pyramidal neurons in mouse somatosensory cortex are independent of apical dendrite bundling. *Journal of Neuroscience*, *27*, 11473. doi:10.1523/jneurosci.1182-07.2007.

Kubota, Y., Kondo, S., Nomura, M., Hatada, S., Yamaguchi, N., Mohamed, A. A., Karube, F., Lübke, J., & Kawaguchi, Y. (2015). Functional effects of distinct innervation styles of pyramidal cells by fast spiking cortical interneurons. *eLife*, *4*, e07919. doi:10.7554/eLife.07919.

Landauer, R. (1961). Irreversibility and heat generation in the computing process. *IBM Journal of Research and Development*, *5*, 183–191. doi:10.1147/rd.53.0183.

Larkum, M. E., Senn, W., & Lüscher, H.-R. (2004). Top-down dendritic input increases the gain of layer 5 pyramidal neurons. *Cerebral Cortex*, *14*, 1059–1070. doi:10.1093/cercor/bhh065.

Laughlin, S. B., de Ruyter van Steveninck, R. R., & Anderson, J. C. (1998). The metabolic cost of neural information. *Nature Neuroscience*, *1*, 36–41. doi:10.1038/236.

Lee, S.-H., Marchionni, I., Bezaire, M., Varga, C., Danielson, N., Lovett-Barron, M., Losonczy, A., & Soltesz, I. (2014). Parvalbumin-positive basket cells differentiate among hippocampal pyramidal cells. *Neuron*, *82*, 1129–1144. doi:10.1016/j.neuron.2014.03.034.

Leff, H. S., & Rex, A. F. (2002). *Maxwell's Demon 2: Entropy, Classical and Quantum Information, Computing*. Boca Raton: CRC Press. doi:10.1201/9781420033991.

Lent, C. S., Orlov, A. O., Porod, W., & Snider, G. L. (2019). *Energy Limits in Computation: A Review of Landauer's Principle, Theory and Experiments*. Cham, Switzerland: Springer. doi:10.1007/978-3-319-93458-7.

Levitin, L. B. (1998). Energy cost of information transmission (along the path to understanding). *Physica D: Nonlinear Phenomena*, *120*, 162–167. doi:10.1016/S0167-2789(98)00051-7.

Lobaugh, J., & Voth, G. A. (1996). The quantum dynamics of an excess proton in water. *Journal of Chemical Physics*, *104*, 2056–2069. doi:10.1063/1.470962.

Magistretti, P. J., & Allaman, I. (2015). A cellular perspective on brain energy metabolism and functional imaging. *Neuron*, *86*, 883–901. doi:10.1016/j.neuron.2015.03.035.

Malik, R., Dougherty, K. A., Parikh, K., Byrne, C., & Johnston, D. (2016). Mapping the electrophysiological and morphological properties of CA1 pyramidal neurons along the longitudinal hippocampal axis. *Hippocampus*, *26*, 341–361. doi:10.1002/hipo.22526.

Marx, M., & Feldmeyer, D. (2012). Morphology and physiology of excitatory neurons in layer 6b of the somatosensory rat barrel cortex. *Cerebral Cortex*, *23*, 2803–2817. doi:10.1093/cercor/bhs254.

Marx, M., Qi, G., Hanganu-Opatz, I. L., Kilb, W., Luhmann, H. J., & Feldmeyer, D. (2015). Neocortical layer 6b as a remnant of the subplate - a morphological comparison. *Cerebral Cortex*, *27*, 1011–1026. doi:10.1093/cercor/bhv279.

McKhann, G. M., D'Ambrosio, R., & Janigro, D. (1997). Heterogeneity of astrocyte resting membrane potentials and intercellular coupling revealed by whole-cell and gramicidin-perforated patch recordings from cultured neocortical and hippocampal slice astrocytes. *Journal of Neuroscience*, *17*, 6850–6863. doi:10.1523/jneurosci.17-18-06850.1997.

Mergenthaler, P., Lindauer, U., Dienel, G. A., & Meisel, A. (2013). Sugar for the brain: the role of glucose in physiological and pathological brain function. *Trends in Neurosciences*, *36*, 587–597. doi:10.1016/j.tins.2013.07.001.

Mounier, A., Georgiev, D., Nam, K. N., Fitz, N. F., Castranio, E. L., Wolfe, C. M., Cronican, A. A., Schug, J., Lefterov, I., & Koldamova, R. (2015). Bexarotene-activated retinoid X receptors regulate neuronal differentiation and dendritic complexity. *Journal of Neuroscience*, *35*, 11862–11876. doi:10.1523/jneurosci.1001-15.2015.

Niell, C. M., & Stryker, M. P. (2010). Modulation of visual responses by behavioral state in mouse visual cortex. *Neuron*, *65*, 472–479. doi:10.1016/j.neuron.2010.01.033.

Nieuwenhuys, R. (1994). The neocortex. *Anatomy and Embryology*, *190*, 307–337. doi:10.1007/bf00187291.

Page, C. H. (1981). Higher functions of cerebral cortex. In P. D. Sturkie (Ed.), *Basic Physiology* (pp. 134–147). New York: Springer. doi:10.1007/978-1-4613-8081-8_9.

Palmer, L. M., Shai, A. S., Reeve, J. E., Anderson, H. L., Paulsen, O., & Larkum, M. E. (2014). NMDA spikes enhance action potential generation during sensory input. *Nature Neuroscience*, *17*, 383. doi:10.1038/nn.3646.

Pathak, D., Guan, D., & Foehring, R. C. (2016). Roles of specific Kv channel types in repolarization of the action potential in genetically identified subclasses of pyramidal neurons in mouse neocortex. *Journal of Neurophysiology*, *115*, 2317–2329. doi:10.1152/jn.01028.2015.

Plenio, M. B., & Vitelli, V. (2001). The physics of forgetting: Landauer's erasure principle and information theory. *Contemporary Physics*, *42*, 25–60. doi:10.1080/00107510010018916.

Polsky, A., Mel, B. W., & Schiller, J. (2004). Computational subunits in thin dendrites of pyramidal cells. *Nature Neuroscience*, *7*, 25–60. doi:10.1038/nn1253.

Porod, W., Grondin, R. O., Ferry, D. K., & Porod, G. (1984). Dissipation in computation. *Physical Review Letters*, *52*, 232–235. doi:10.1103/PhysRevLett.52.232.

Rakic, P. (2009). Evolution of the neocortex: a perspective from developmental biology. *Nature Reviews Neuroscience*, *10*, 724–735. doi:10.1038/nrn2719.

Rockland, K., & DeFelipe, J. (2018). *Why Have Cortical Layers? What Is the Function of Layering? Do Neurons in Cortex Integrate Information Across Different Layers?*. Lausanne: Frontiers Media. doi:10.3389/978-2-88945-660-4.

Sagawa, T., & Ueda, M. (2008). Second law of thermodynamics with discrete quantum feedback control. *Physical Review Letters*, *100*, 080403. doi:10.1103/PhysRevLett.100.080403.

Sagawa, T., & Ueda, M. (2010). Generalized Jarzynski equality under nonequilibrium feedback control. *Physical Review Letters*, *104*, 090602. doi:10.1103/PhysRevLett.104.090602.

Santamaría-Pang, A., Hernandez-Herrera, P., Papadakis, M., Saggau, P., & Kakadiaris, I. A. (2015). Automatic morphological reconstruction of neurons from multiphoton and confocal microscopy images using 3D tubular models. *Neuroinformatics*, *13*, 297–320. doi:10.1007/s12021-014-9253-2.

Schwindt, P., O'Brien, J. A., & Crill, W. (1997). Quantitative analysis of firing properties of pyramidal neurons from layer 5 of rat sensorimotor cortex. *Journal of Neurophysiology*, *77*, 2484–2498. doi:10.1152/jn.1997.77.5.2484.

Scott, A. C. (2005). *Encyclopedia of Nonlinear Science*. New York: Routledge. doi:10.4324/9780203647417.

Sengupta, B., Stemmler, M. B., & Friston, K. J. (2013). Information and efficiency in the nervous system—a synthesis. *PLOS Computational Biology*, *9*, e1003157. doi:10.1371/journal.pcbi.1003157.

Sengupta, P. (2013). The laboratory rat: relating its age with human's. *International Journal of Preventive Medicine*, *4*, 624–630.

Shipp, S. (2007). Structure and function of the cerebral cortex. *Current Biology*, *17*, R443–R449. doi:10.1016/j.cub.2007.03.044.

Squire, L. R., Genzel, L., Wixted, J. T., & Morris, R. G. (2015). Memory consolidation. *Cold Spring Harbor perspectives in biology*, *7*, a021766. doi:10.1101/cshperspect.a021766.

Staiger, J. F., Loucif, A. J. C., Schubert, D., & Möck, M. (2016). Morphological characteristics of electrophysiologically characterized layer Vb pyramidal cells in rat barrel cortex. *PLOS ONE*, *11*, e0164004. doi:10.1371/journal.pone.0164004.

Street, S. (2016). Neurobiology as information physics. *Frontiers in Systems Neuroscience*, *10*. doi:10.3389/frsyns.2016.00090.

Street, S. (2020). Upper limit on the thermodynamic information content of an action potential. *Frontiers in Computational Neuroscience*, *14*. doi:10.3389/fncom.2020.00037.

Tripathy, S. J., Burton, S. D., Geramita, M., Gerkin, R. C., & Urban, N. N. (2015). Brain-wide analysis of electrophysiological diversity yields novel categorization of mammalian neuron types. *Journal of Neurophysiology*, *113*, 3474–3489. doi:10.1152/jn.00237.2015.

Tyan, L., Chamberland, S., Magnin, E., Camiré, O., Francavilla, R., David, L. S., Deisseroth, K., & Topolnik, L. (2014). Dendritic inhibition provided by interneuron-specific cells controls the firing rate and timing of the hippocampal feedback inhibitory circuitry. *Journal of Neuroscience*, *34*, 4534. doi:10.1523/jneurosci.3813-13.2014.

Ueta, Y., Otsuka, T., Morishima, M., Ushimaru, M., & Kawaguchi, Y. (2013). Multiple layer 5 pyramidal cell subtypes relay cortical feedback from secondary to primary motor areas in rats. *Cerebral Cortex*, *24*, 2362–2376. doi:10.1093/cercor/bht088.

Vetter, P., Roth, A., & Häusser, M. (2001). Propagation of action potentials in dendrites depends on dendritic morphology. *Journal of Neurophysiology*, *85*, 926–937. doi:10.1152/jn.2001.85.2.926.

Wible, G. C. (2013). Hippocampal physiology, structure and function and the neuroscience of schizophrenia: a unified account of declarative memory deficits, working memory deficits and schizophrenic symptoms. *Behavioral Sciences*, *3*, 298–315. doi:10.3390/bs3020298.

Yang, W., & Sun, Q.-Q. (2018). Circuit-specific and neuronal subcellular-wide E-I balance in cortical pyramidal cells. *Scientific Reports*, *8*, 3971–3971. doi:10.1038/s41598-018-22314-9.

Zhou, P., Burton, S. D., Snyder, A. C., Smith, M. A., Urban, N. N., & Kass, R. E. (2015). Establishing a statistical link between network oscillations and neural synchrony. *PLOS Computational Biology*, *11*, e1004549. doi:10.1371/journal.pcbi.1004549.

Zhu, J. J. (2000). Maturation of layer 5 neocortical pyramidal neurons: amplifying salient layer 1 and layer 4 inputs by Ca^{2+} action potentials in adult rat tuft dendrites. *Journal of Physiology*, *526*, 571–587. doi:10.1111/j.1469-7793.2000.00571.x.